

Research article

Effects of milling time on the development of porosity in Cu by the reduction of CuO

Laura N. Guevara ¹, Christopher B. Nelson ¹, Gaurav Hans ¹, Cammie L. Atwater ², and Mark A. Atwater ^{1,*}

¹ Department of Applied Engineering, Safety and Technology, Millersville University, Millersville, PA, USA

² Department of Health Science, University of Bridgeport, Bridgeport, CT, USA

* **Correspondence:** Email: mark.atwater@millersville.edu; Tel: 1-717-871-7217.

Abstract: Microscale and nanoscale CuO was dispersed in Cu using room temperature high-energy ball milling over time intervals of 5, 30, 60, 120, and 240 min. These samples were then annealed under a reducing atmosphere for 1 h at temperatures of 400, 600, 800 and 1000 °C to create porosity by the reduction of the entrained oxides. Increases in porosity exceeding 40% were achieved using intermediate milling times and annealing temperatures. When considered cumulatively, the most effective processing conditions were a milling time of 30 min and expansion at 800 °C, but variations exist within each sample type. The complex relationship between milling time and annealing temperature is investigated in terms of particle size, morphology and microstructure. The findings indicate that room temperature milling is more efficient at producing porosity than comparable cryogenic methods, and this may enable industrial scaling of the process.

Keywords: microporous; metallic foam; intraparticle expansion; mechanical alloying; metal powder

Abbreviations

SEM	Scanning Electron microscopy
XRD	X-ray Diffraction
ANOVA	Analysis of Variance

1. Introduction

Porous materials in nature have very unique properties, such as high energy absorption, low specific weight, high gas permeability, buoyancy, and good strength with low density. As expected, man-made materials with the same properties are desired. Porous polymers have been successfully designed to achieve these properties and widely adopted, but porous metals have proven to be more challenging to produce, especially in the solid state. The numerous benefits possible with metallic foams have sustained interest, despite the challenges [1]. Porosity can be divided into two categories: closed cell and open cell. Closed cell foams have pores separated by cell walls which gives them higher strength and are typically used for structural applications. On the other hand, open cell metal foams, sometimes called metallic sponges, have interconnected pores and are mainly used in functional applications [1,2].

The mechanical properties of a porous metal correspond to the ones of the bulk metal, and they are dependent on the density and qualities of the cellular structure (e.g., cell connectivity, cell roundness and diameter, distribution, etc.) [2,3,4]. Functional properties of metal foams are also determined by their cellular character, and, generally speaking, metal foams are of interest for applications involving high surface area, acoustic and thermal management, filtration and others [5,6,7]. Metal foams are also incorporated in composite sandwich panels used in applications where high bending and buckling resistance are needed with minimal weight, including aerospace structures and the hulls of ships [8,9].

Despite satisfying a variety of technological needs, metal foams have seen limited adoption. This is primarily limited by lingering challenges with production. Manufacturing processes for metal foams can also be divided into two main groups: liquid state foaming and solid state foaming. Common methods for liquid state foaming include adding gas bubbles directly into the molten metal or by mixing gas-releasing agents into the melt [5]. Solid state methods typically utilize powder metals, and popular methods include the use of a template or entrapped gas to create porosity [1,10]. Aluminum foams have enjoyed markedly more development than other metals due to their ease of liquid state processing and the diverse means to achieve it [11,12]. Because of its potential use in biomedical and aerospace applications, titanium has also been thoroughly studied, but it cannot be readily processed by liquid state methods and instead has been the focus of many solid state processing methods [10]. Although there are numerous ways porous metals can be made in the solid state (e.g., [1,10,13]), few are practical at large scale, can be equally applied to a variety of metals, and that do not require specialized, often time-consuming, methods.

Current methods for solid state foaming that rely on powder create porosity between particles. Recent reports [14,15,16] on foaming Cu by the reduction of CuO have demonstrated that microscale porosity can be created within individual particles using a relatively simple process of distributing oxides through ball milling. The greatest obstacle in the method to-date is the use of cryogenic processing which is impractical to scale. An alternative method for preparing the Cu powder by surface oxidation was recently described [17], and initial efforts to use room temperature milling produced even higher porosity than comparable cryogenic methods. The limit to that work was that Cu began plating out on the milling vial due to the higher temperature and increased ductility. This work overcomes that challenge by using a surfactant and explores the pertinent process parameters to

achieve maximum porosity with the simplest methodology. To achieve this, pore volume is compared to various factors influenced by milling time and foaming temperature. Because this process generates expandable powder, the characteristics of the powder are of central interest.

2. Materials and Method

Copper-copper oxide (Cu-CuO) mixtures were prepared using a Spex 8000D high-energy ball mill with a ball-to-powder mass ratio of 10:1. Each sample consisted of 5 g of powder in a 49:1 atomic ratio of Cu:CuO. Elemental powders of copper (99%, <75 μm), copper(II) oxide (98%, <10 μm), and copper(II) oxide nanoparticles (<50 nm) were used to make the mixtures, and 1 wt% stearic acid (reagent grade, 95%) was added as a surfactant to eliminate cold welding. All were obtained from Sigma-Aldrich and used without modification. Two sets of separate mixtures were milled for 5, 30, 60, 120, and 240 min, in that order, without cleaning the milling vial in between runs to reduce contamination from the vial and milling media. Since little to no cold welding occurred, no significant remnant of material was included in the subsequent millings. One set of mixtures was milled using the micron-sized CuO (hereafter referred to as “Regular” CuO) and the other set was milled with nanoscale CuO (hereafter referred to as “Nano” CuO). All powders were handled and stored in a glove box under argon (<1 ppm O₂, <1 ppm H₂O) and the same high-purity Ar atmosphere was present in the vial during milling.

To quantify the change in porosity of the different mixtures, approximately 50 mg of each mixture was compacted at 2 GPa in a 3 mm diameter tungsten carbide die. To foam sample compacts, the furnace was preheated to the desired temperature (400, 600, 800, or 1000 °C) and samples were pushed into the hot zone. Once they reached temperature they were held for 1 h and retracted to cool at ambient temperature. The entire process was conducted under 200 sccm flow of 5% H₂ (bal. Ar) in a 50 mm diameter single zone tube furnace (Across International). Volumetric density was calculated before and after annealing the compacts. The change in density was used to calculate the percent change in porosity of each sample. The sample data points correspond to the average of at least three compacts annealed under the same conditions. Error bars indicate one standard deviation in the data. The same conditions were repeated under nitrogen to collect hardness values for annealed compacts.

Compacts were mounted in epoxy and prepared with a Pace Technologies Nano-1000T metallographic polisher using a progression of abrasives, culminating with 1200 grit SiC. These samples were observed with a Meiji MT7500 optical microscope to assess the porosity in annealed compacts. As-milled powders were compacted, annealed (except the as-milled condition) and similarly prepared before conducting Vickers hardness testing with a Leco LM-100 microindenter. A minimum of 10 indents at 50 g with a 10 sec dwell time were used to determine hardness. Error bars indicate one standard deviation in the data. As-milled samples were analyzed by X-ray diffraction (XRD) using a PANalytical X'Pert Pro MPD diffractometer with Cu anode (Cu K α wavelength: 1.54 Å). Scherrer estimates of crystallite size were calculated by whole-pattern fitting in X'Pert Highscore software, and values are the average of the first five Cu peaks in the pattern. Scanning electron microscopy (SEM) was performed with a JEOL 7400F microscope operated at 3 kV. Dilatometry was performed for two samples of each composition milled for 30 min with a Linseis L74 optical dilatometer using a heating rate of 10 °C/min to 1000 °C in a mixture of Ar (226 sccm)

and H₂ (90 sccm). Samples for dilatometry were prepared identically to those for isothermal annealing and volumetric density measurements. Particle size analysis was conducted in isopropyl alcohol with a Malvern Mastersizer S and values represent the average of five runs. Statistical analysis was performed in Minitab 17 software using an α level of 0.5, and pooled standard deviation was used in interval plots.

3. Results and Discussion

Various methods were employed to determine the amount of porosity produced and the factors influencing the outcome. The development of porosity is described in Section 3.1 as a function of milling time and foaming temperature. Particle characteristics are described in Section 3.2 with regard to microstructure and morphology. In Section 3.3, the influence of processing parameters on final porosity is analyzed. Section 3.4 provides discussion on the observed process-property relationships.

3.1. Development of Porosity

To determine the effects of milling time and annealing temperature, Cu was milled with Regular (<10 μm) and Nano (<50 nm) CuO. As shown in Figure 1, the two mixtures behave differently during annealing. The Regular CuO samples consistently achieve the highest levels of porosity at 800 $^{\circ}\text{C}$. Figure 1A shows that samples milled for 5 min have the lowest overall porosity (<10%), and the samples milled for 30 min have the highest porosities (>40% at 800 $^{\circ}\text{C}$). The data in Figure 1B reveal that samples annealed at 400 $^{\circ}\text{C}$ have the lowest porosity overall, followed by 600 $^{\circ}\text{C}$ and 1000 $^{\circ}\text{C}$. In general, the maximum porosity is reached after 30 min of milling and additional milling time does not improve the amount of porosity or lowers it.

The Nano CuO samples are not as uniform in their response. As shown in Figure 1C, increasing temperature results in a monotonic rise in porosity for the mixture milled for 5 min to a modest maximum of 21%. The sample milled for 30 min reaches its 35% maximum at 600 $^{\circ}\text{C}$, with lower porosity at higher temperatures. Samples milled for 60, 120 and 240 min all reach maximum porosity at 800 $^{\circ}\text{C}$. The sample milled for 240 min has a higher maximum (36%) than 60 min and 120 min (23%), which behave similarly throughout the temperature range. In Figure 1D it is shown that 30 min of milling results in the most porosity for all temperatures except 800 $^{\circ}\text{C}$, which is highest for the samples milled for 240 min. Notably, the greatest increase in porosity for the 60 min milled samples (35%) is achieved at a lower temperature, and samples at each time interval above and below this are relatively inactive (porosity increases of <5%).

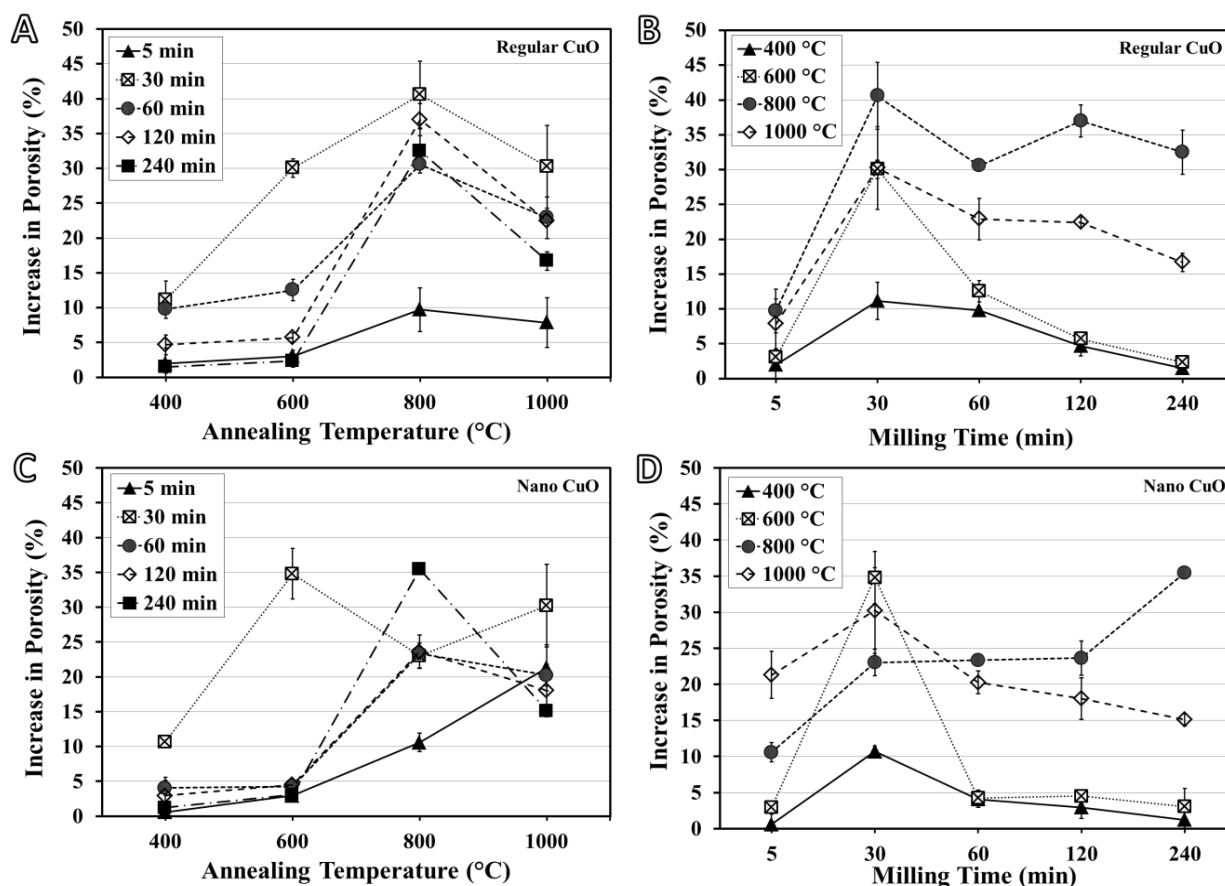


Figure 1. Porosity developed in Regular CuO as a function of (A) annealing temperature and (B) milling time, and porosity developed in Nano CuO as a function (C) annealing temperature and (D) milling time.

To examine porosity in sample compacts, they were foamed, mounted and polished. The polished cross-sections of select samples foamed at 800 °C are shown in Figure 2. Because porosity is developed within particles, there exists a combination of inter-particle porosity from incomplete consolidation and intra-particle porosity from the foaming process. Optical microscopy is limited in the detail it can reveal about the microscale pores created using oxide reduction, but it is significantly faster and simpler than focused ion beam (FIB) cross-sectioning, and pore morphology can be described using it [16], though with less resolution. This work seeks to determine total porosity, so the exact pore morphology is not of primary interest. Nonetheless, in the Regular CuO sample milled for 5 min (Figure 2A) it can be seen that large, inter-particle porosity is visible, but little to no intra-particle pores appear. In the Regular CuO sample milled for 30 min (Figure 2B) a uniform distribution of small pores is observable and in the 60 min sample (Figure 2C) these are fewer and concentrated at particle boundaries (consistent with the differences in porosity shown in Figure 1B). A similar trend is seen in the Nano CuO samples. Little intra-particle porosity appears after milling for 5 min (Figure 2D), but more can be seen in the 30 min sample (Figure 2E) and is similarly distributed in the sample milled for 60 min (Figure 2F). For all samples, mechanical polishing is limited in its ability to resolve such fine porosity, but the method is useful to broadly assess the structure.

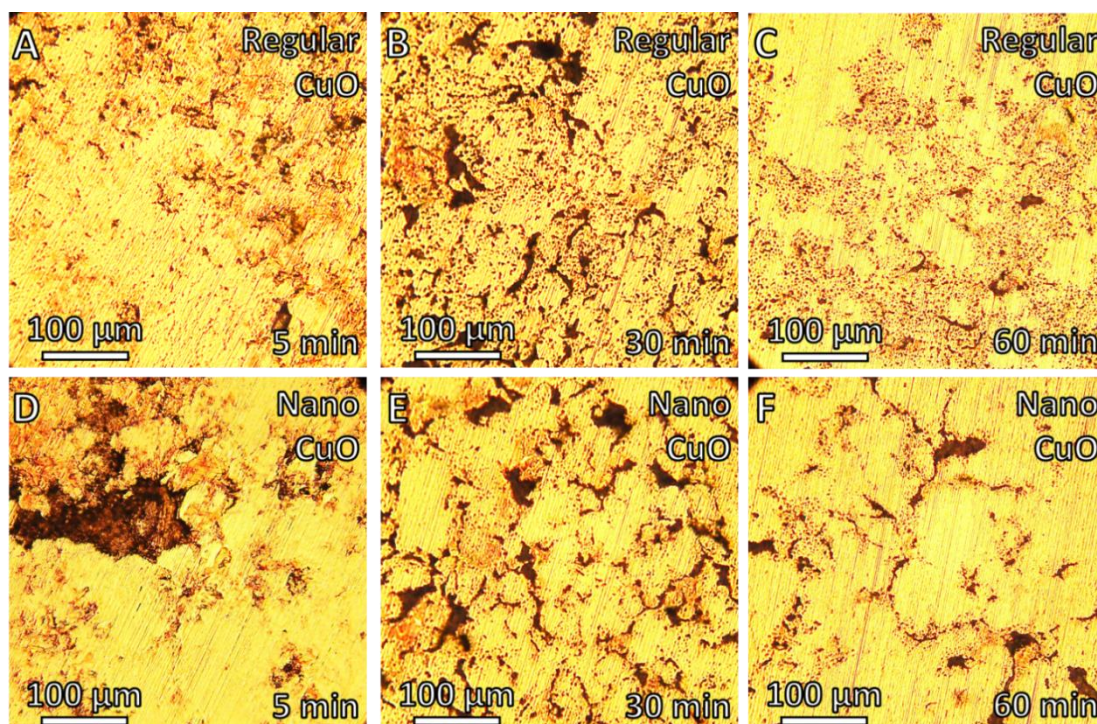


Figure 2. After annealing at 800 °C, samples of Regular CuO milled for (A) 5 min, (B) 30 min, and (C) 60 min, and samples of Nano CuO milled for (D) 5 min, (E) 30 min, and (F) 60 min were examined using optical microscopy.

To quantify the process of expansion, dilatometry was performed on samples of each composition milled for 30 min, and the results are shown in Figure 3. The curves represent the instantaneous change in height with temperature, and as shown, the Regular and Nano CuO have similar trends, but the Regular CuO expands more and maintains its dimensions over a greater temperature range. The Nano CuO begins expanding at a slightly higher temperature, but once expansion begins, the rate is similar. Both samples contracted significantly after reaching a maximum between 650 and 700 °C. The contraction is attributed to a combination of sintering and coalescence/percolation of pores within the particles, and it is expected that the maximum achieved at 800 °C is the consequence of this contraction. It should also be noted that the process for dilatometry is different from that used to measure expansion geometrically. Specifically, the annealed samples were placed into a pre-heated furnace, not ramped to the final temperature as conducted in the dilatometer.

The dilatometer measures height optically, but it is clear from the images that expansion occurs in all directions (note the gap changes between the sample (left) and Al₂O₃ standard (right) in Figure 3). The expansion process was recorded and a video comparing samples of Regular and Nano CuO is available in Supplementary Material. Three images from that video are provided for each sample. On the left side of Figure 3 are images of a Regular CuO compact at the beginning (I), point of maximum expansion (II), and end of the run (III), and these are replicated for the Nano CuO sample on the right side (see Figure 3, center, for the corresponding points labeled on the curve).

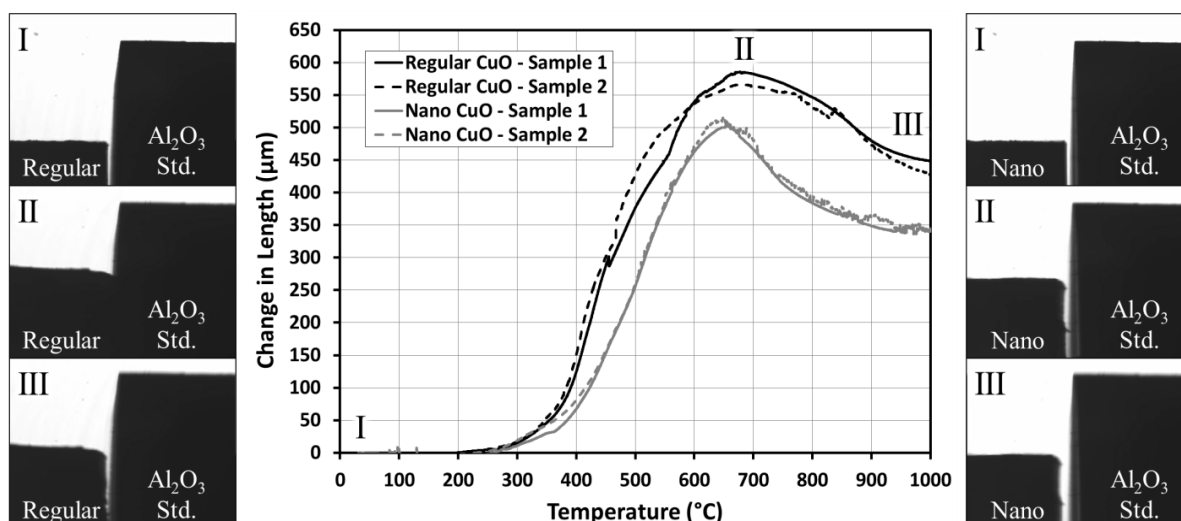


Figure 3. Optical dilatometry was performed on two samples each of Regular and Nano CuO compositions. The optical images collected during dilatometry are shown (I) at the beginning of the run, (II) at maximum expansion, and (III) at maximum temperature (1000 °C). A video corresponding to these tests is provided in Supplemental Material.

3.2. Particle Characteristics

Because oxide reduction and intra-particle expansion is a powder-based process, the properties of the powder have an important influence on the resulting structure. Various factors are active simultaneously, including the size and distribution of oxides, the microstructure of the Cu and the overall particle size and morphology. Key microstructural features will be determined by a combination of grain size and particle reinforcement in these materials, and each may affect the ability to create compacts, the resistance to expansion, etc. To determine these properties, the approximate grain size, hardness, the particle size, and oxygen content were analyzed.

XRD was performed to compare the microstructural refinement in the Regular and Nano CuO materials, and the resulting patterns are shown in Figure 4A and Figure 4B, respectively. There is little difference between the two, and CuO peaks were only visible (but nearly imperceptible) in the Regular CuO sample milled for 5 min, which indicates that the small volume fraction of oxide is rapidly dispersed throughout the structure of the Cu. The refinement of crystallite size was estimated according to Scherrer analysis [18], and the average of the first five peaks of the pattern are presented in Figure 4C. The estimations are nearly identical for Regular and Nano CuO at all milling times. Lower milling times are more likely to be inaccurate because of a distribution of grain sizes and strain broadening which are not accounted for in this estimation, but the comparison of the two CuO types indicates similar microstructural development.

To provide a more direct measurement of the structure, microindentation was performed on the as-milled samples and those annealed at the primary foaming temperatures (600 °C and 800 °C), and the results are given in Figure 5. The Regular and Nano CuO are very similar in hardness over the range of milling times, reaching a steady state of 1.4–1.6 GPa after 60 min of milling, with the Nano CuO samples consistently having higher hardness by approximately 0.2 GPa. The as-milled hardness

values follow a similar trend to the estimated grains sizes (Figure 4C), but the hardness values are lower than predicted. The measured hardness of 1.5 GPa is estimated for a 50 nm grain size [19], even if not including the Orowan strengthening provided a dispersed phase [20]. After annealing at 600 °C, there is a notable drop in hardness for lower milling times (60 min and less), but it is much less for samples milled for 120 min and 240 min (~0.2 GPa), and the Nano CuO sample at 240 min was measured to be slightly harder than the as-milled mixture (but within error). Improved thermal stability can be achieved by a distribution of fine particles [21], which can be produced by longer milling times. A notable correlation between the softening effect at 600 °C after 30 min of milling and pore formation should be noted. Specifically, for samples foamed at 600 °C, those milled for 30 min displayed the greatest amount of expansion, and the total increase in porosity follows an inverse relationship to hardness. The exception is 5 min, which is likely not sufficient to thoroughly mix the oxides throughout the Cu. The general trend after annealing at 600 °C is an increase in hardness with milling time, but after annealing at 800 °C, shorter milling times are slightly harder than longer milling times. It is likely that all milling times have relatively similar microstructures (oxides and grains coarsen appreciably) as the temperature exceeds the ability of the oxide particles to stabilize a small grain size. As discussed below, shorter milling times have a higher oxygen/oxide concentration, which may account for the small (0.2 MPa) difference.

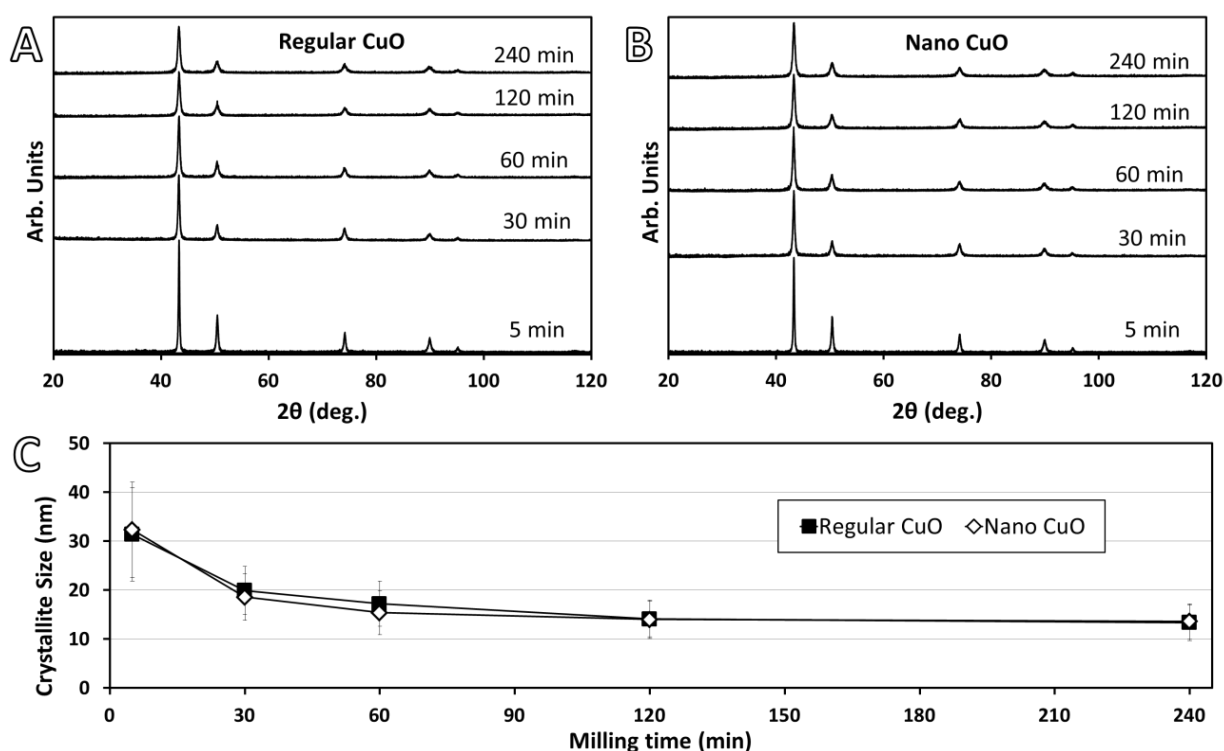


Figure 4. XRD was performed to track the microstructural refinement in the samples by analyzing the peak shapes for each milling time in (A) Regular CuO and (B) Nano CuO samples. Peak fitting was applied to estimate the grain size by Scherrer analysis and (C) the mean peak sizes are given for each composition and milling time.

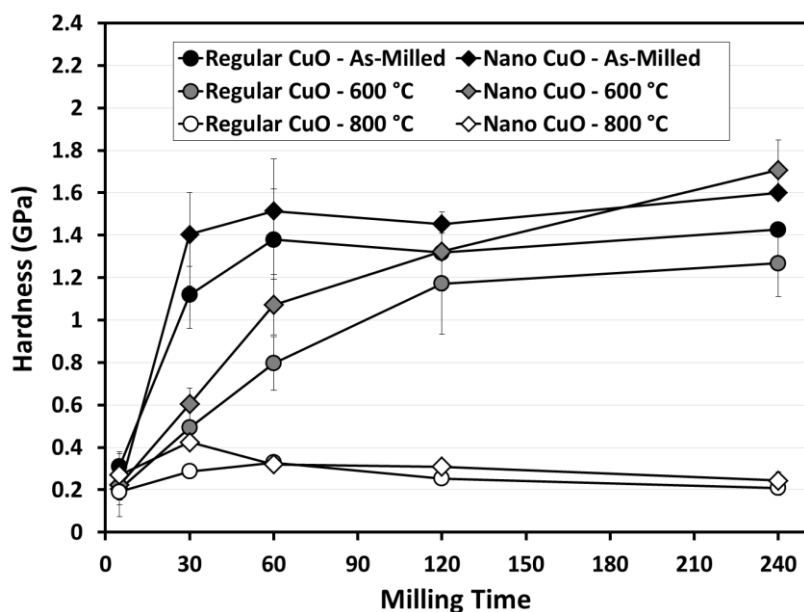


Figure 5. Hardness measured by microindentation of Regular and Nano CuO samples in the as-milled and annealed conditions. Annealing was performed in nitrogen to suppress foaming.

The increase in porosity was determined as a volumetric expansion of powder compacts, but the measured compacts are dependent on the initial powder characteristics. Any bulk component processing will also be effected by powder characteristics, so SEM was performed on particles of each sample to determine the general morphology of the particles, and particle size analysis was performed to acquire a quantitative distribution of sizes. As shown in the SEM images in Figure 6A and Figure 6E, the particles are predominately plate-like in shape throughout the studied milling times. The particle size distributions for Regular CuO (Figure 6B) and Nano CuO (Figure 6C) show a similar size distribution for the two compositions, as both have a greater proportion of small particles ($<10\ \mu\text{m}$) after 5 min of milling, and the vast majority of the particles are between 10 and $100\ \mu\text{m}$. As summarized in Figure 6D, notable differences can be summarized by trends in the small particles (10th percentile, or 10% of particles below the listed value), the median size (50th percentile, or 50% above/below) and the largest sizes (90th percentile, or 90% below). For instance, Regular and Nano CuO samples milled for 30 min have the largest overall sizes by a small margin for all milling times except for the Regular CuO sample milled for 60 min, which shows a significant volume percentage of very large particles ($150\text{--}300\ \mu\text{m}$). The Regular CuO has larger particle sizes than the Nano CuO at each milling time. At the 10th and 50th percentile the difference is typically less than $10\ \mu\text{m}$. At the 90th percentile it is larger, especially at milling times of 60 min and greater, indicating the Regular CuO has a relatively small number of large particles that account for a considerable proportion of the total volume. In general, the planar morphology of the particles may actually inhibit expansion due to the close proximity of the oxides to free surfaces, and pores will rapidly percolate. Because a fine distribution of particles is created, this does not inhibit foaming, but it may be problematic with larger oxide particles.

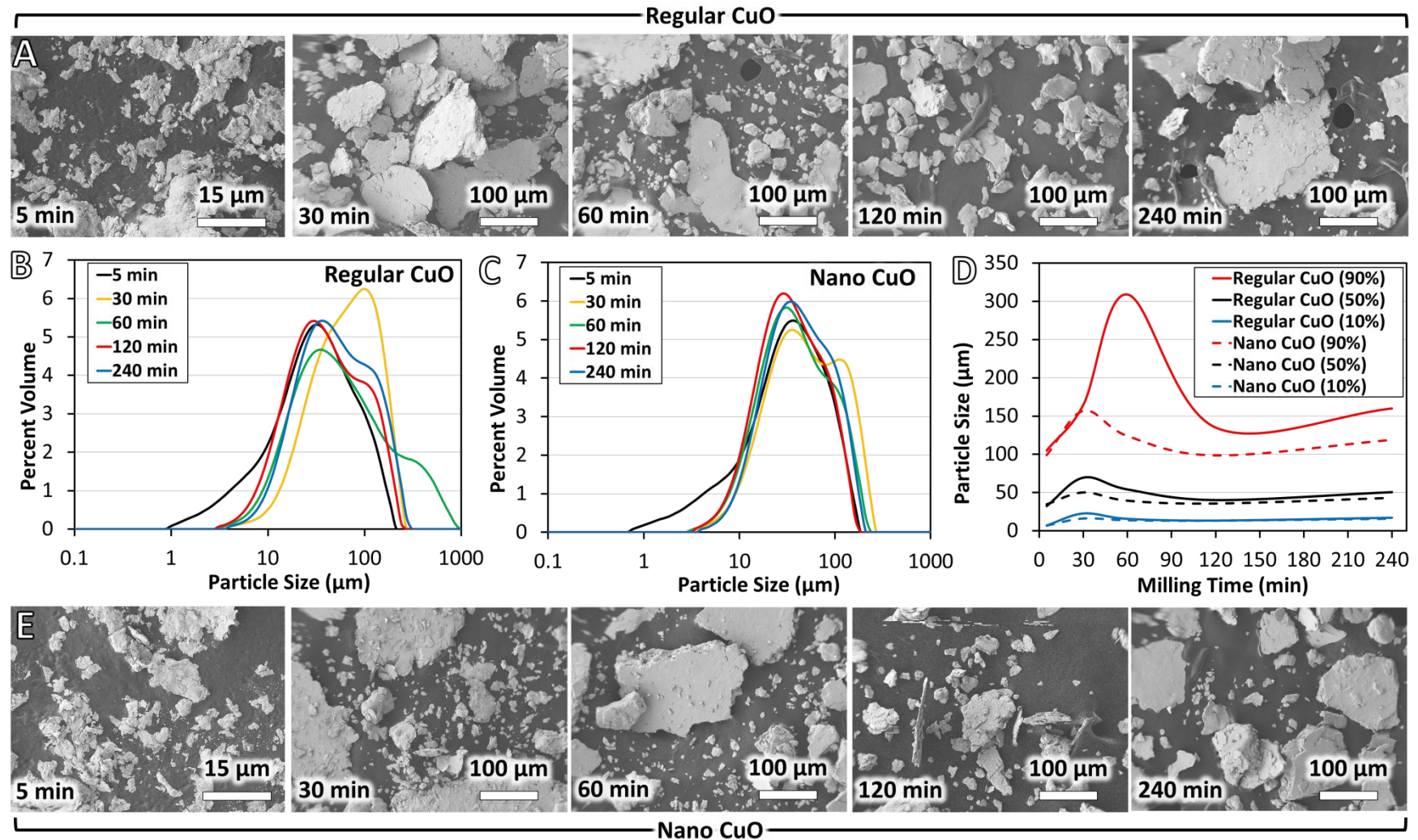


Figure 6. The development of particle size and morphology at each milling time. (A) SEM of Regular CuO powder after milling at the indicated times, (B) particle size distributions for Regular CuO samples, (C) particle size distribution for Nano CuO samples, (D) particle sizes at the 10th, 50th and 90th percentiles for Regular (solid lines) and Nano (dashed lines) CuO, and (E) SEM of Nano CuO powder after milling for the indicated times. Note the different scale bar used on the 5 min sample for Regular and Nano CuO SEM.

Individual particles were also examined after milling for 30 min and annealing at 600 °C and 800 °C, and the resulting morphology is shown in Figure 7. The planar morphology is less evident after foaming, indicating that significant expansion has occurred. Surface pores are clearly visible for all samples, and as the porosity at the surface increases, the roughness of the surface around those pores also increases. The Nano CuO annealed at 600 °C exhibits the least amount of porosity at the surface, but as seen in Figure 1D, this condition also had the greatest increase in porosity as measured volumetrically. Although Nano CuO annealed at 800 °C has a lower porosity, the pore quantity at the surface is greater. This may indicate a greater rate of coalescence and percolation which will limit total porosity. The surface porosity for Regular CuO appears similar between 600 °C and 800 °C, but the 800 °C samples exhibited greater porosity (see Figure 1B).

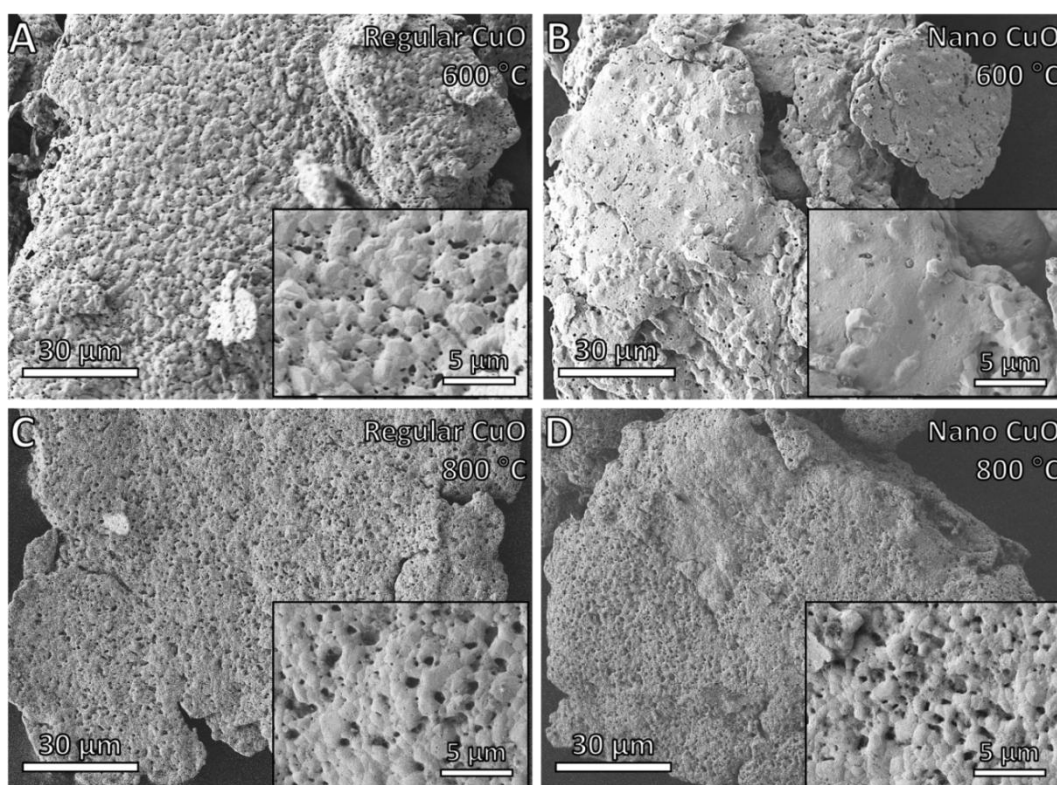


Figure 7. Particle morphology for (A) Regular and (B) Nano CuO after 30 min of milling and annealing at 600 °C and (C) Regular and (D) Nano CuO after 30 min of milling and annealing at 800 °C for 1 h in 5% H₂ (bal. Ar).

In prior work [15,17], it was determined that oxygen content (as CuO) is critical to the outcome of the foaming process. This is controlled by the type and quantity of powders added at the beginning of the milling process. Here, the oxide addition was specified at 2 at%, but the nominally pure Cu had no oxygen specification, nor does the manufacturer provide documentation of it. With its dark, reddish-brown appearance, the as-received Cu powder was evidently oxidized and will increase the overall oxygen concentration. Oxygen-free high-conductivity Cu (OHFC) powder can be used to reduce the initial oxygen concentration, and therefore, allow better accuracy when adding CuO separately, but cost is greater. Also, with the addition of stearic acid and prolonged milling times, the

loss of oxygen during milling as a result of temperature or reactions with the surfactant was a concern. As shown in Table 1, the oxygen content started 2 at% higher than the specified addition of CuO. The addition of 1 wt% stearic acid ($C_{18}H_{36}O_2$, molar mass of 284.48 g/mol) will only add about 0.03 at% oxygen (oxygen is ~11.3 wt% of the stearic acid molecule) to the Cu-CuO mixture (63.866 g/mol for the mixture, nominal). This indicates that the additional oxygen is most likely from the Cu powder. As milling time increases, the oxygen content decreases, indicating that some conversion of the CuO is occurring. The oxygen content is very similar for Regular and Nano CuO, and the oxygen content drops slightly more between 5 and 30 min (0.6–0.7 at%) than between 30 and 240 min (0.6 at%). This suggests that the system is most affected in the earlier stages of milling. Possible causes for oxygen loss in the powder include the thermal and chemical decomposition of CuO as a consequence of the high temperatures encountered during milling and availability of C and H to react with the oxides to form otherwise stable products (e.g., CO_2). Additionally, the remaining oxygen concentration does not guarantee that it is available as distributed CuO particles, and it may be present in a form that does not contribute to foaming.

Table 1. Variation in oxygen concentration in milled powders at various intervals.

Sample	Milling Time (min)	Oxygen Content (at%)
Regular CuO	5	4.04
	30	3.36
	240	2.70
Nano CuO	5	3.97
	30	3.34
	240	2.85

3.3. Influence of Process Parameters

Because there are many factors simultaneously affecting the outcome of the foaming process, the relationship and significance of these factors was analyzed. First, the collective results for increase in porosity were examined using a one-way ANOVA for each sample type as a function of milling time and annealing temperature, and the interval plots for the data are given in Figure 8. These identify overall trends in the foaming process, and indicate conditions where statistically different results exist. For example, the Regular CuO samples exhibit the highest porosity after 30 min of milling (Figure 8A) and 800 °C annealing (Figure 8B), but the only milling times that are statistically significant in their difference from 30 min are 5 min and 240 min. Regular CuO samples foamed at 800 °C are significantly different from all other temperatures. The Nano CuO samples follow similar trends as the Regular CuO with maximum increases in porosity occurring at 30 min (Figure 8C) and 800 °C (Figure 8D). The material milled for 30 min is significantly different from all others, but foaming at 800 °C is not significantly different from 1000 °C.

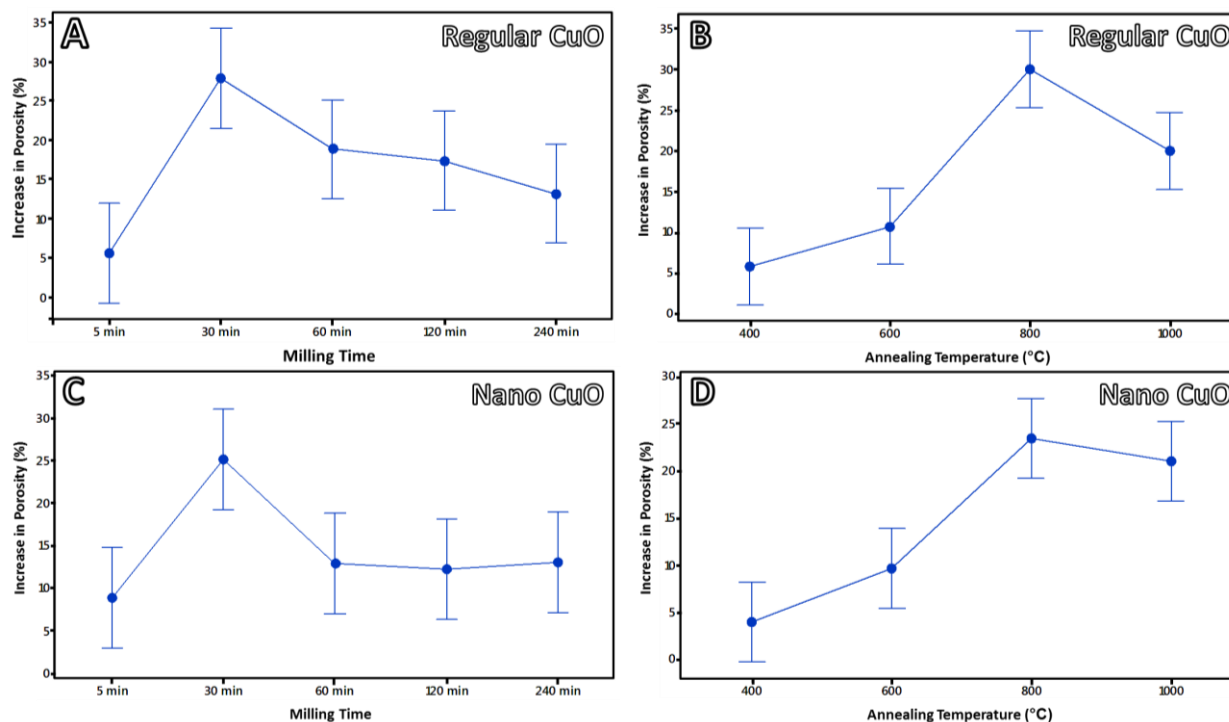


Figure 8. Interval plots of cumulative data for Regular CuO shown as (A) percent increase in porosity as a function of milling time, and (B) percent increase in porosity as a function of annealing temperature, and Nano CuO for (C) percent increase in porosity as a function of milling time, and (D) percent increase in porosity as a function of annealing temperature. Data points represent mean values, and analysis was performed using a 95% confidence interval (error bars).

To provide a basic map for optimizing foaming, contour plots were created for the Regular and Nano CuO samples using milling time, annealing temperature and percent increase in porosity as the x, y and z variables, respectively (see Figure 9). There are notable similarities between the two materials. For instance, both display a general trend of increasing porosity for lower milling times and increasing temperature, and both have isolated areas of maximum porosity. For Regular CuO (Figure 9A), this occurs around 750–850 °C for milling times of 25–35 min. For Nano CuO there are two locations. The first is at temperatures from 550–700 °C and milling times of 20–35 min, and the second is at temperatures from 775–900 °C and milling times of 200–240 min (the maximum time studied). The Nano CuO consistently produces lower overall porosity than Regular CuO. These plots are indicative of the trends, but they do not account for other variables that might be encountered. For instance, it is indicated that no expansion will occur at 500 °C and 240 min of milling for either sample type, but foaming (10% max) will occur at 400 °C and 600 °C. This is counterintuitive to the requirement of heat to drive the process, and is not consistent with dilatometry, where a monotonic increase in porosity is observed until at least 700 °C (though processed somewhat differently). The contour plots are valuable in visualizing the trends, and with more complete data can be an improved and useful tool. Other factors, such as relationship between milling time and initial density, the initial

density and increase in porosity were also examined, but no notable correlation to the formation of porosity was found.

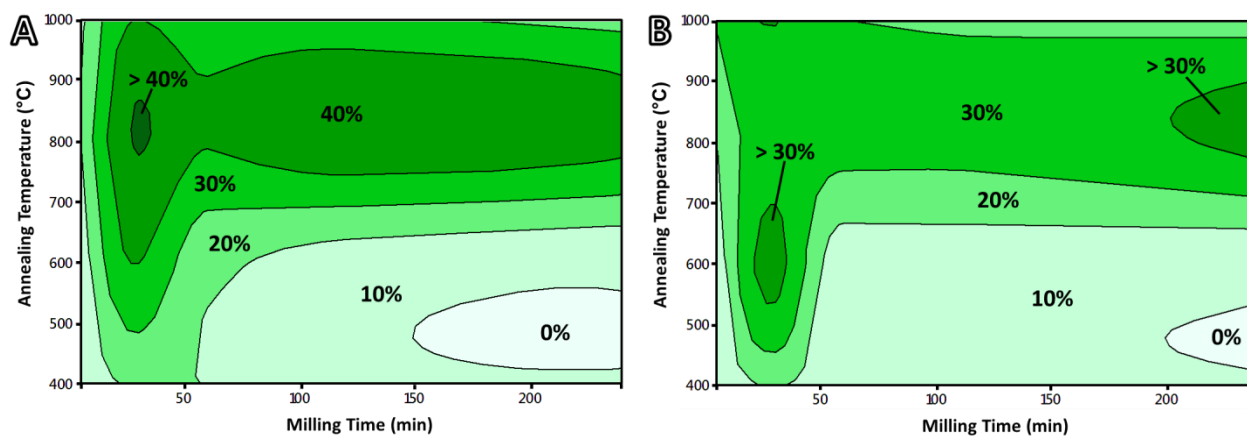


Figure 9. Contour maps of (A) Regular CuO and (B) Nano CuO showing the variation in porosity with processing conditions. Percentages indicate the maximum within that contour.

3.4. Process-Property Relationships

The ability to create porosity within individual particles may have important technological consequences, as it provides a feedstock that can be used in any other powder metallurgy process. Understanding fundamental factors in the development of the powder and resulting metallic foams is a critical step in producing a reliable result. Several important advancements are made as part of this work. In prior foaming work in the Cu-CuO system [14,15], samples were processed by cryogenic high-energy ball milling. This work provides the first systematic description of this foaming technique using room temperature milling. In a recent study [17], room temperature milling was investigated for surface oxidized Cu-CuO powders as a potential means to achieve a commercially viable process. There it was found that by milling at room temperature greater porosity can be achieved in less time (30 min vs 4 h of cryogenic milling) and with greater simplicity. The disadvantage was that milling times greater than 30 min resulted in extensive cold welding and could not be studied. Here, stearic acid was used to eliminate cold welding and allow longer milling times. This is accompanied by particular attention to powder characteristics, as this material is expected to be used in powder-based processes and those properties are important.

As evidenced by the contour maps (Figure 9), the relationship between processing and foaming is complex. Unlike the only similar solid state method, gas entrapment and expansion (e.g., [22]), which uses pressurized Ar pores, oxide reduction is not clearly linked to temperature as the foaming step is an interplay of temperature, atmosphere and oxide characteristics. Nonetheless, certain global statements can be made. For instance, intermediate milling times are most effective. This may be attributed to a combination of higher oxygen content, coarser oxide size (higher initial pore size), lower hardness and increased particle size. Specifically, when referring back to Figure 1, it can be noted that porosity typically drops at 1000 °C. Dilatometry reveals this is related to the contraction

of the material after maximum porosity is reached, likely as a consequence percolation and sintering. This is an important result because it indicates that an intermediate foaming time may also be most effective, similar to the milling time and annealing temperatures. Longer milling times also typically resulted in less porosity, with the most significant deviation from this trend being the Nano CuO samples annealed at 800 °C, which show an increasing trend in porosity with milling time. While it is not certain through the present analyses, it may be related to the combination of very small, well-distributed oxide particles that strengthen the matrix too much to allow expansion at lower temperatures (600 °C and below) but which result in faster percolation and sintering at 1000 °C. The precise role of oxides (size, spacing, etc.) will be a topic of further study. The general results are encouraging, as they demonstrate that long milling times, annealing times and high annealing temperatures are not necessary and that the use of a surfactant does not interrupt the foaming process as studied here. These factors are crucial for potential scaling of the process.

The challenge in developing the oxide reduction and intraparticle expansion technique is that it is a very dynamic process. The size, distribution and quantity of oxide particles affect the microstructure and the development of porosity. For example, in samples cryogenically milled for 4 h and annealed at 600 °C, it was found that the reduction of oxides starts from the surface and progresses to the center of the particles [15], resulting in a nanocrystalline core with nano- to microscale grains and pores where the oxides have been reduced. The microstructural development, then, is an integral part of the foaming process. The purpose of using nanoscale oxides in this work was to examine the importance of the oxide size and, if necessary, to allow a finer dispersion than typically produced in short, room temperature milling processes. The more numerous and smaller the oxide particles are, the more effective they are at reducing grain growth and retaining a higher-strength matrix [23], which may counteract the expansion process. By tracking the hardness of the samples at varying milling times and after annealing without foaming, it was found that at 800 °C the materials have softened significantly, and this is also the temperature at which the process was found to result in the highest porosity when these materials and processing conditions are considered collectively (i.e., Figure 8). Despite some differences, the two oxide types generally behave similarly, with the Regular CuO resulting in higher porosity, and therefore making it a better choice both for cost and performance.

4. Conclusions

The mechanical milling process used to produce expandable powder feedstock by oxide reduction and expansion has been successfully demonstrated using room temperature milling with the addition of stearic acid. Microscale and nanoscale CuO were studied over a range of milling times and foaming temperatures, and in most cases, the two responded similarly. The micron CuO resulted in higher total porosity (41%) than the nanoscale CuO (36%). An intermediate milling time (30 min) and foaming temperature (800 °C) were found to be the optimum conditions on average, but some variation existed within the data. By considering the effects of milling on the powder size, microstructure, and morphology, it was determined that intermediate milling times result in larger particles with a softer matrix that are preferable in foaming. After 30 min of milling median particle sizes (50th percentile) were similar and maximized for both Regular and Nano CuO. Regular CuO

contained larger particles overall, and after 60 min of milling the 90th percentile was notably higher without significant deviation between the two compositions at lower percentiles, indicating a small number of very large particles. Higher temperatures reduce the hardness of the Cu-CuO mixtures and allow more efficient expansion, but the response is dependent on milling time. As milling time increased, the hardness retained after annealing at 600 °C also increased, even though the as-milled values were similar. This interplay of variables was summarized with processing maps (contour plots) that indicate intermediate conditions of milling and temperature produce the greatest increase in porosity, and the creation of pore volume does not benefit by starting with nanoscale CuO.

Acknowledgements

The authors are grateful to the organizations which assisted through characterization facilities and analysis: The University of Delaware Keck Center for Advanced Microscopy and Microanalysis (SEM), Franklin and Marshall University (XRD), Pennsylvania State University Materials Characterization Laboratory (particle size analysis), Luvak Laboratories (oxygen analysis), and Tom Luckenbaugh, Roger Welsh and Brady Butler for performing dilatometry (Army Research Laboratory). This work was supported by the National Science Foundation CAREER Award #1555016.

Conflict of Interest

All authors declare no conflicts of interest in this paper.

References

1. Kennedy A (2012) Porous Metals and Metal Foams Made from Powders, In: Kondoh K, *Powder Metallurgy*, Rijeka, Croatia: InTech Europe, 31–46.
2. Garc ía-Moreno F (2016) Commercial applications of metal foams: their properties and production. *Materials* 9: 85.
3. Ashby MF (1983) Mechanical properties of cellular solids. *Metall Trans A* 14: 1755–1769.
4. Banhart J, Baumeister J (1998) Deformation characteristics of metal foams. *J Mater Sci* 33: 1431–1440.
5. Banhart J (2001) Manufacture, characterisation and application of cellular metals and metal foams. *Prog Mater Sci* 46: 559–632.
6. Banhart J (2007) Metal Foams—from Fundamental Research to Applications, In: Raj B, Ranganathan S, Rao KBS, et al., *Frontiers in the Design of Materials*, India: Universities Press.
7. Lin JH, Luo DL, Chen SL, et al. (2016) Control interfacial microstructure and improve mechanical properties of TC4-SiO_{2f}/SiO₂ joint by AgCuTi with Cu foam as interlayer. *Ceram Int* 42: 16619–16625.
8. Elzey DM, Wadley HNG (1999) Open-die forging of structurally porous sandwich panels. *Metall Mater Trans A* 30: 2689–2699.

9. Vancheeswaram R, Queheillalt DT, Elzey DM, et al. (2001) Simulation of the creep expansion of porous sandwich structures. *Metall Mater Trans A* 32: 1813–1821.
10. Dunand DC (2004) Processing of Titanium Foams. *Adv Eng Mater* 6: 369–376.
11. Banhart J (2006) Metal Foams: Production and Stability. *Adv Eng Mater* 8: 781–794.
12. Banhart J (2013) Light-Metal Foams—History of Innovation and Technological Challenges. *Adv Eng Mater* 15: 82–111.
13. Lefebvre LP, Banhart J, Dunand DC (2008) Porous Metals and Metallic Foams: Current Status and Recent Developments. *Adv Eng Mater* 10: 775–787.
14. Atwater MA, Darling KA, Tschopp MA (2014) Towards Reaching the Theoretical Limit of Porosity in Solid State Metal Foams: Intraparticle Expansion as a Primary and Additive Means to Create Porosity. *Adv Eng Mater* 16: 190–195.
15. Atwater MA, Darling KA, Tschopp MA (2016) Solid-State Foaming by Oxide Reduction and Expansion: Tailoring the Foamed Metal Microstructure in the Cu–CuO System with Oxide Content and Annealing Conditions. *Adv Eng Mater* 18: 83–95.
16. Atwater MA, Darling KA, Tschopp MA (2016) Synthesis, characterization and quantitative analysis of porous metal microstructures: Application to microporous copper produced by solid state foaming. *AIMS Mater Sci* 3: 573–590.
17. Atwater MA, Luckenbaugh TL, Hornbuckle BC, et al. (2017) Advancing commercial feasibility of intraparticle expansion for solid state metal foams by the surface oxidation and room temperature ball milling of copper. *J Alloy Compd* 724: 258–266.
18. Cullity BD, Stock SR (2001) *Elements of X-Ray Diffraction (3rd)*, Upper Saddle River, NJ: Prentice Hall.
19. Chen J, Lu L, Lu K (2006) Hardness and strain rate sensitivity of nanocrystalline Cu. *Scripta Mater* 54: 1913–1918.
20. Bacon DJ, Kocks UF, Scattergood RO (1973) The effect of dislocation self-interaction on the Orowan stress. *Philos Mag* 28: 1241–1263.
21. Andrievski R (2014) Review of thermal stability of nanomaterials. *J Mater Sci* 49: 1449–1460.
22. Dunand D, Teisen J (1998) Superplastic foaming of titanium and Ti-6Al-4V. *Mat Res Symp Proc* 521: 231.
23. Nes E, Ryum N, Hunderi O (1985) On the Zener drag. *Acta Metall* 33: 11–22.



AIMS Press

© 2017 Mark A. Atwater, et al. licensee AIMS Press. This is an open access article distributed under the terms of the Creative Commons Attribution License (<http://creativecommons.org/licenses/by/4.0>)